

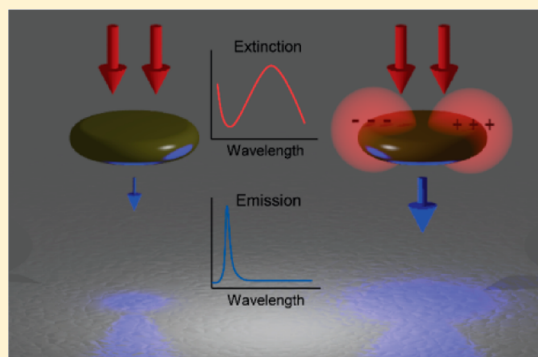
Plasmon-Enhanced Two-Photon Absorption in Photoluminescent Semiconductor Nanocrystals

Brandon C. Marin,^{†,‡} Su-Wen Hsu,^{†,‡} Li Chen,[§] Ashley Lo,[†] Darwin W. Zwissler,[†] Zhaowei Liu,[§] and Andrea R. Tao^{*,†}

[†]NanoEngineering Department and [§]Department of Electrical and Computer Engineering, University of California, San Diego, 9500 Gilman Drive MC 0448, La Jolla, California 92093-0448, United States

Supporting Information

ABSTRACT: In this work, we demonstrate the two-photon fluorescence of covellite-phase copper sulfide nanodisks and investigate the role of the surface plasmon resonance on emission. Using selenium doping, we blue-shift the plasmon resonance toward the two-photon absorption edge. We observed a 3-fold enhancement of emission in these samples and report two-photon action cross sections that are an order of magnitude greater than conventional fluorophores. These nanomaterials offer a novel “all-in-one” platform for engineering plasmon–exciton coupling in the absence of a physical or chemical interface.



KEYWORDS: near-infrared plasmonics, multiphoton absorption, copper sulfide, nonlinear photonics, enhanced light–matter interactions, plasmon resonance tuning

Two-photon-absorbing (2PA) inorganic nanoparticles that are capable of upconverting near-infrared (NIR) light have the potential to enable a wide range of biophotonic applications, ranging from fluorescence imaging in live tissue^{1–4} to photodynamic therapy⁵ and clinical diagnostics.^{6,7} Semiconductor quantum dots composed of metal chalcogenides^{1,8,9} and Au nanoparticles^{10–13} are the two main types of colloidal solid-state nanoparticles that are currently being explored as contrast agents for in vivo two-photon-induced emission (2PE) imaging and spectroscopy. A major advantage of utilizing these types of solid-state nanoparticles is the ability to probe live tissue with much larger penetration depths, since NIR light encounters less intrinsic scattering within tissue than visible light. Bright 2PA nanoparticles that operate within the biological tissue transparency window (630–1300 nm) are particularly desirable for reaching deep tissue for carrying out optical sectioning or achieving three-dimensional imaging.⁷ In comparison to conventional organic dyes that are used in 2PE measurements, inorganic nanoparticles also exhibit reduced photobleaching and increased photostabilities.⁶ Their chemical surfaces are also readily modified with specific chemistries for increased biocompatibility, cell or tumor targeting, and prolonged circulation upon systemic delivery into an organism.^{14,15}

The synthesis of bright nanoparticle probes with large 2PE action cross sections is still a major challenge. One strategy to increase the brightness of 2PA nanoparticles is to excite a localized surface plasmon resonance (LSPR) that serves as a virtual state for NIR photon absorption (Figure 1).¹⁶ For example, Au nanorods support a LSPR that is polarized along

the longitudinal nanorod axis and can be excited between 700 and 1000 nm, depending on the nanorod aspect ratio.¹⁷ 2PA is generated by plasmon excitation in the NIR, while fluorescence in the visible range is generated by radiative decay from intraband transitions of Au. However, the 2PE action cross sections of Au nanorods and nanoparticles are inherently limited by the low fluorescence quantum efficiencies of Au, which is in the range of 10^{-4} .¹⁸ Alternatively, organic dyes have also been demonstrated to exhibit enhanced 2PE when in the close vicinity of a plasmonic Ag or Au nanoparticle,^{19,20} but coupling between the LSPR of the nanoparticle and the electronic transition of the dye in this multicomponent system is weak.²¹

The ability to excite an LSPR for enhanced 2PA properties and to obtain strong exciton emission from a single nanoparticle would be highly desired for 2PE measurements. Highly doped semiconductor nanocrystals (SNCs) have the potential to serve as these “all-in-one” type nanoparticles. We and others have recently demonstrated that SNCs that possess a large number of free carriers can support LSPR excitation in the NIR and exciton generation in the same structure.^{22–24} For example, Cu_{2-x}S is a self-doped semiconductor where the introduction of Cu vacancies in the crystal lattice produces hole carriers. Cu_{2-x}S SNCs exhibit an LSPR mode in the NIR range, well below the band-gap energy (1.2 eV for Cu_2S).²²

Received: January 15, 2016

Published: March 14, 2016

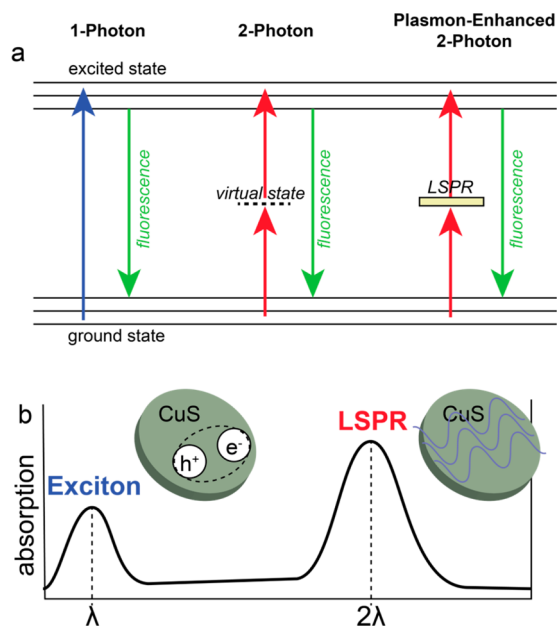


Figure 1. (a) Schematic of the electronic transitions for 2PE. (b) Schematic of the absorbance profile for plasmon-assisted 2PA.

Advantageously for 2PA, the LSPR of these SNCs can be explicitly tuned within the NIR to mid-IR wavelength ranges. We have characterized how Cu_{2-x}S SNCs respond to changes in carrier density, including the effects of carrier density tuning on near-field confinement and plasmonic coupling.²⁵ We have also observed shape-dependent LSPRs for SNCs by demonstrating that Cu_{2-x}S nanodisks possess both in-plane and out-of-plane dipolar LSPRs.^{24,26} CuS (covellite) nanodisks, in particular, exhibit a strong in-plane dipolar mode that dominates the NIR extinction spectrum.

While the fluorescent and plasmonic properties of highly doped SNCs have been studied extensively in recent years,^{22,25,26} very little work has been done to investigate the 2PA properties of these materials. In particular, very little is known about how LSPR excitation and tuning can affect the 2PA cross sections of colloidal nanomaterials. In this work, we demonstrate the 2PA and 2PE properties of CuS nanodisks. We show that the wavelength of the in-plane LSPR mode is critical to 2PE enhancement and that 2PA can be tuned on- and off-resonance to observe these effects. Our results show that for 2PA that is tuned near the LSPR excitation wavelength, the 2PE intensity observed from CuS nanodisks can be increased by a 3-fold enhancement.

EXPERIMENTAL METHODS

Chemicals. 1-Octadecene ($\text{C}_{18}\text{H}_{36}$, 90%), oleylamine ($\text{C}_{18}\text{H}_{35}\text{NH}_2$, 70%), and sulfur powder (S, 98.98%) were purchased from Sigma-Aldrich. Cupric nitrate hemipentahydrate ($\text{Cu}(\text{NO}_3)_2 \cdot 2.5\text{H}_2\text{O}$, 98%) and chloroform (CHCl_3 , 99.25%) were purchased from Fisher Chemical. Selenium powder (Se, 99.99%) was purchased from Alfa Aesar. All reagents were used as purchased.

CuS Nanodisk Synthesis. A solvent mixture of oleylamine and 1-octadecene was prepared in a 1:3 ratio, respectively. A 0.0928 g amount of copper nitrate (0.4 mmol) was dissolved in 4 mL of solvent mixture by sonication, yielding a dark blue 0.1 M Cu precursor solution. For CuS nanodisks, 0.0192 g of sulfur powder (0.6 mmol) was added to the precursor solution.

The mixture was then heated to 160 °C in an oil bath for 30 min, forming a dark green solution. To remove excess oleylamine and 1-octadecene, 4 mL of ethanol was added and the mixture was centrifuged at 3K rpm for 5 min. The precipitate was then removed, redispersed in chloroform, and centrifuged at 7.5K rpm for 7.5 min to remove any byproducts. This final centrifugation was repeated twice. The purified precipitate was then dispersed in 4 mL of chloroform for use and analysis. For Se-doped CuS nanodisks, a 0.6 mmol total mixture of Se:S powder was used in lieu of 0.0192 g of sulfur powder. The ratio of Se:S was varied to control the concentration of dopant in the final product.

Materials Characterization. Se:S content was determined using energy dispersive X-ray spectroscopy (EDX). EDX spectra were obtained using a Philips XL30 ESEM with an Oxford EDX detector attachment coupled with Inca software. Samples were prepared by drop-casting onto a clean silicon support. The EDX detector was calibrated using the K_{α} peak of a Cu standard. Spot size, magnification, beam accelerating voltage, and process time were all kept constant to ensure accuracy in measurement. Relative errors in measurements are summarized in [Supplementary Figure S14](#). Powder X-ray diffraction (XRD) spectra were taken using a Rigaku RU200B diffractometer coupled with MDI Datascan5 software. A step size of 0.02° and a dwell time of 1.0 s were used at a 100 kV operating voltage. Samples were dried and deposited on a clean glass slide for measurement. An FEI Tecnai G2 Sphera running a LaB_6 filament at 200 kV was used for transmission electron microscopy (TEM) micrographs. A Gatan Ultrascan 1000 UHS CCD camera running Gatan Digital Micrograph was used for imaging. TEM samples were prepared by drop-casting nanodisks dispersed in chloroform onto an air–water interface. Carbon-film Cu grids (200 mesh) were then dip-coated in the dispersion.

Optical Characterization. Optical extinction spectra were taken using a PerkinElmer Lambda-1050 UV–vis–NIR spectrophotometer with a three-detector module. The samples were dispersed in chloroform using a 1 cm quartz cuvette. Scans were performed from 250 to 2000 nm. Photoluminescence spectra were acquired using a Princeton Instruments Acton SP2300 monochromator coupled to a Nikon Eclipse LV100 upright microscope. A Kimmon Koha 20 mW 325 nm He–Cd laser was used as an excitation source. Samples were prepared by drop-casting onto a clean glass slide. For 2PE measurements, a Leica SP5 confocal microscope with a Leica HyD detector was used. This system was coupled to a Spectra Physics Mai Tai HP tunable laser. The excitation wavelength of the Mai Tai HP was varied from 690 to 1040 nm with an average power of 2.5 mW and pulsed at 100 fs through a 10× Leica objective. For sampling, a colloidal solution of nanodisks in chloroform was sealed in a glass chamber. For direct sample comparison, signal intensity was normalized for particle concentration, which was determined using reported methods.²⁷ Chambers were sealed using 65 μL of 15 × 15 mm frame seals by Bio-Rad. Mean 2PE emission intensity values for varied excitation wavelengths were determined by integrating the detector signal over a specified and fixed wavelength range. This collected range was 400–650 nm, which covers the range of the emission spectra for all samples and is described further in the [Supporting Information](#) (Section S1). Molar absorptivity (α) values were calculated directly from particle concentration and absorbance. Laser power measurements were performed using an Ophir Vega hand-held laser power meter.

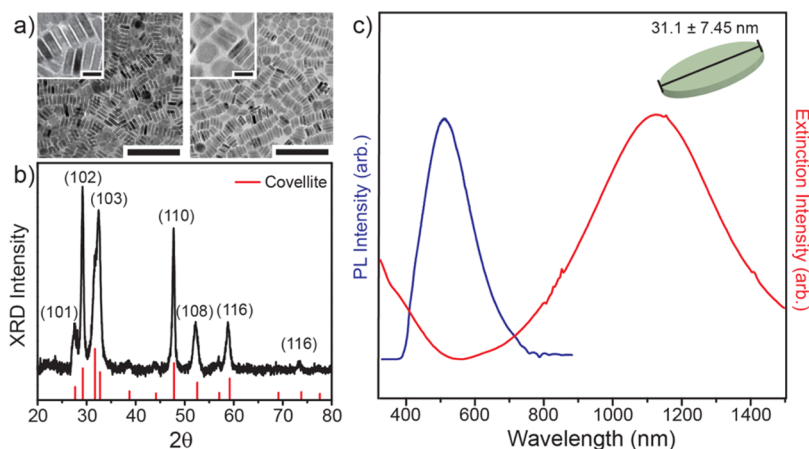


Figure 2. CuS optical properties: (a) Typical TEM micrographs of CuS nanodisks (left) and Se-doped CuS nanodisks (right); scale bars are 150 nm. Insets are zoomed-in images; inset scale bars are 20 nm. (b) Typical XRD spectra of CuS nanodisks with highlighted diffraction pattern. (c) Photoluminescence emission spectra and extinction spectra for CuS.

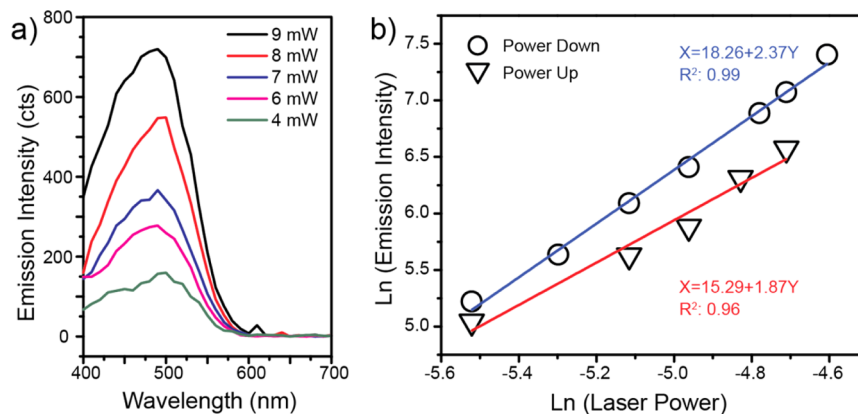


Figure 3. Nonlinear CuS emission: (a) 2PE spectra of CuS at various laser powers; (b) log–log plot showing the power-square dependence of emission. Laser power was incrementally increased (Power Up) and decreased (Power Down) to acquire two separate fits for comparison.

RESULTS AND DISCUSSION

CuS nanodisks were synthesized using solvent-based methods as described in the [Experimental Methods](#) section. An excess of sulfur powder was used to ensure the formation of the stoichiometric CuS (covellite) phase, as opposed to the $\text{Cu}_{7.2}\text{S}_4$ (digenite) phase, which preferentially occurs at higher Cu:S ratios.²⁶ [Figure 2a](#) shows a TEM micrograph of a dispersion of undoped (left) and Se-doped (right) CuS nanodisks using the solvent-based method, which yielded particles with an average diameter of 31.14 ± 7.45 nm with an aspect ratio of 4.54 ± 1.51 . The diameters and aspect-ratio distributions of individual samples are fully listed in [Table S1](#). The powder XRD spectrum of CuS nanodisks is shown in [Figure 2b](#), highlighting the characteristic diffraction peaks of the covellite phase. CuS is a p-type semiconductor that exhibits semimetal behavior.²⁸ Furthermore, it exhibits absorptive and emissive optical responses. [Figure 2c](#) plots an overlay of the photoluminescence emission ($\lambda_{\text{ex}} = 325$ nm) and the extinction spectrum for a typical colloidal CuS nanodisk sample dispersed in chloroform. The extinction peak in the NIR is a maximum at $\lambda_{\text{LSPR}} = 1125$ nm and is attributed to a strong in-plane dipole mode. The onset of the absorption edge can be observed at ca. 400 nm and is the result of excitonic absorption due to quantum confinement and a direct band gap.²⁹ The Stokes-shifted photoluminescence emission maximum occurs at $\lambda_{\text{F}} = 505$ nm. λ_{LSPR} in undoped

CuS nanodisks occurs at well over double the wavelength of the absorption edge, which enables 2PA.

To determine whether these CuS are capable of nonlinear absorption, we carried out 2PE measurements using femto-second-pulsed laser excitation at $\lambda_{\text{ex}} = 855$ nm. CuS nanodisk samples were prepared by drop-casting and drying the dispersion onto a clean glass slide. These samples exhibit a well-defined emission peak centered at ca. $\lambda_{\text{F}} = 500$ nm ([Figure 3a](#)). The line shape and location of this peak is in close agreement with the single-photon fluorescence measurements in [Figure 2c](#). In order to demonstrate that this emission is the result of 2PA, we measured the fluorescence emission intensity with respect to the power of the excitation source. While single-photon absorption is expected to give a linear relationship, multiphoton absorption is expected to give rise to a nonlinear relationship between emission intensity and source power.³⁰ For a perfect 2PA process, the emission intensity varies with the square of the source power.³¹ [Figure 3b](#) shows a log–log plot of laser power versus emission intensity. Upon increasing and decreasing laser power, we observed a slope of 1.87 and 2.37, respectively. This is in close agreement with the power-squared dependence (slope = 2) characteristic of a 2PA process.

To study the effect of λ_{LSPR} on 2PE intensities, we modulated the wavelength of λ_{LSPR} by doping the CuS nanodisks with Se. Doping is achieved by direct substitution of S atoms within the covellite lattice with Se atoms. X-ray diffraction measurements

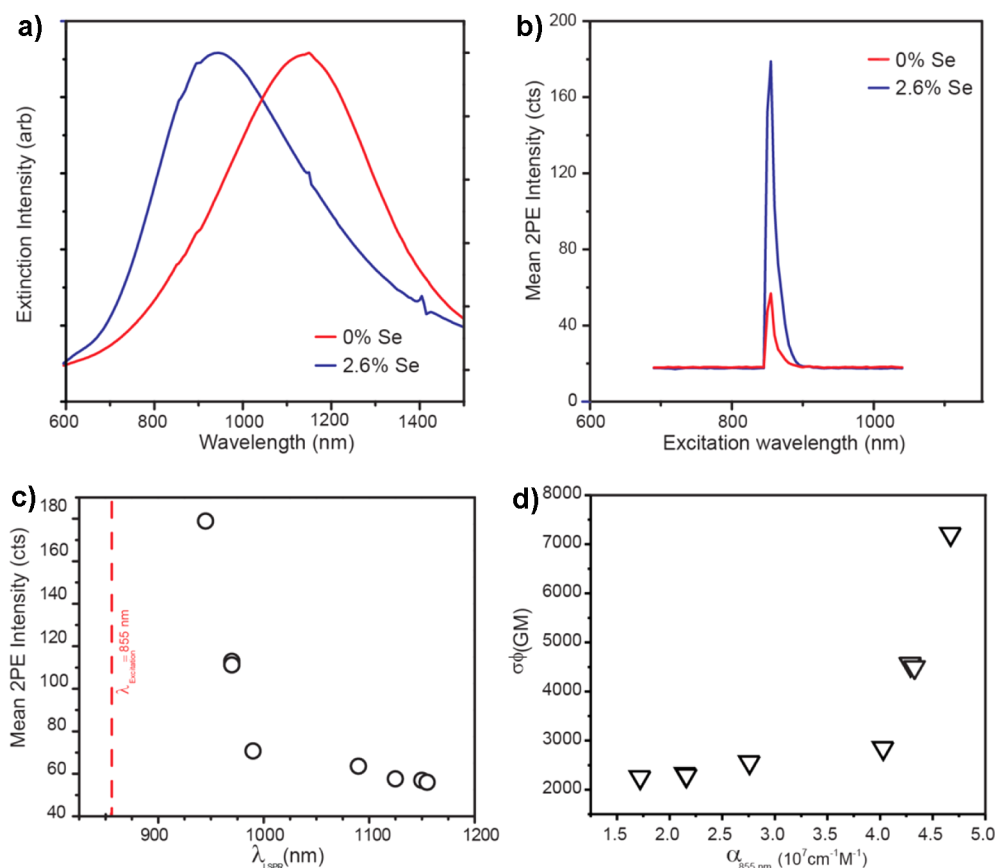


Figure 4. CuS 2PE dependence on plasmon resonance: (a) extinction spectra of 2.6% Se-doped CuS (blue) and undoped CuS (red); (b) mean 2PE intensity as a function of excitation wavelength; (c) dependence of mean 2PE intensity on λ_{LSPR} location; (d) two-photon action cross section as a function of CuS nanodisk molar absorptivity at the excitation wavelength.

show that the crystal structure remains constant and covellite-like, which suggests a 1:1 ratio of Cu to total chalcogen (Figure S3). The extinction spectra for these samples is plotted in Figure 4a, which shows a λ_{LSPR} value of 945 and 1150 nm for doped and undoped samples, respectively. Our results show that the λ_{LSPR} of the in-plane dipole mode can be blue-shifted toward lower wavelengths with increasing Se content. The largest blue-shift in λ_{LSPR} that can be achieved gives $\lambda_{LSPR} = 945$ nm for 2.6 atomic % Se by atomic weight. Increasing the amount of Se content beyond a few percent results in a red-shift in λ_{LSPR} , likely due to poor Se solubility in the CuS lattice (Figure S2).

We then determined whether Se doping results in a change in the 2PA wavelength. Figure 4b shows a plot of the mean 2PE emission intensity with respect to λ_{ex} with a step size of 5 nm. As described in the Experimental Methods section, the mean intensity is the integrated emission signal over a specified wavelength range. This range is fixed for all samples from 400 to 650 nm. This was performed for two samples: (i) an undoped CuS nanodisk dispersion and (ii) a Se-doped CuS nanodisk dispersion with 2.6 atomic % Se, as measured by energy-dispersive X-ray spectroscopy. The two samples show no difference in the λ_{ex} value that gives the maximum 2PE intensity, with $\lambda_{ex} = 855$ nm for both the undoped sample and Se-doped sample. This suggests that Se doping does not affect the absorption edge of the CuS nanodisks.

Next, we measured the mean 2PE emission intensity as a function of λ_{LSPR} for eight different CuS nanodisk samples. These CuS nanodisk samples were synthesized with varying Se content and exhibit in-plane LSPR modes with λ_{LSPR} varying between

945 and 1155 nm. Figure 4c plots the mean 2PE intensity obtained for $\lambda_{ex} = 855$ nm. As the value of λ_{LSPR} begins to approach the value of λ_{ex} , we see that the measured 2PE intensity experiences a dramatic increase. 2PE intensity is maximized as λ_{LSPR} approaches the two-photon absorption edge. This indicates that the increase in emission intensity occurs due to an increase in absorbance, since field enhancement of the fluorescence emission is not expected at these long wavelengths³² (Figure 4c).

To gauge the effect of LSPR excitation on 2PE, we calculated the two-photon action cross sections ($\sigma\phi$) for these CuS nanodisks. $\sigma\phi$ has been used extensively as an effective measure for the magnitude or brightness of two-photon-induced fluorescence emission^{33,34} and is the product of the absolute 2PA cross section (σ) and the fluorescence quantum efficiency (ϕ). We calculated $\sigma\phi$ using previously reported methods^{34,35} and used Lucifer Yellow as a reference fluorophore. This method is described further in the Supporting Information (Section S1). For our samples, $\sigma\phi$ ranged from 2255.2 to 7211.5 Goepfert–Mayer (GM) units, depending on the value of λ_{LSPR} (Table 1). Our results show that higher $\sigma\phi$ values correlate with greater overlap between λ_{LSPR} and λ_{ex} . This range for $\sigma\phi$ is also on the order of previously reported values for solid-state luminescent materials such as CdSe quantum dots and gold nanorods^{1,36} and an order of magnitude above those reported for conventional molecular fluorophores such as Bodipy, DAPI, and rhodamine B.³³

To indicate the relationship between LSPR excitation and 2PE brightness, we plotted $\sigma\phi$ as a function of CuS nanodisk molar absorptivity at 855 nm (α_{855}) (Figure 4d). We calculated

Table 1. Two-Photon Action Cross Sections for Various CuS Samples

sample	λ_{LSPR} (nm)	$\sigma\phi$ (GM)
1	945	7211.5
2	970	4551.7
3	970	4481.5
4	990	2849.7
5	1090	2560.9
6	1125	2322.2
7	1150	2293.9
8	1155	2255.2

α_{855} directly from the extinction spectra for various Se-doped CuS nanodisk samples, as described in the [Experimental Methods](#) section. We observe that $\sigma\phi$ is maximum for our highest obtained value of α_{855} . We also observe that the relationship between $\sigma\phi$ and α_{855} is highly nonlinear and that a critical value of $\alpha_{855} = 4 \times 10^7 \text{ cm}^{-1} \text{ M}^{-1}$ must be reached before the 2PE brightness increases. These higher α_{855} values indicate stronger light absorption, which correlates well with higher 2PE brightness. This is additional evidence that plasmon-assisted absorption plays a role in enhanced absorption, rather than emission.

CONCLUSION

This work demonstrates the nonlinear optical properties of plasmonic covellite CuS nanodisks synthesized by colloidal methods. Furthermore, we probe the effect of LSPR excitation on 2PE by utilizing Se doping to tune the LSPR wavelength. While Se doping is unable to achieve full registry of the LSPR peak with the absorption edge of CuS, we observed a strong enhancement of 2PE emission for samples with higher spectral overlap. This 2PE response is unique in that the SNCs serve as both the plasmonic and photoluminescent components, offering an all-in-one platform for engineering plasmon–exciton coupling in the absence of a physicochemical interface. Furthermore, the 2PE action cross sections indicate that these CuS nanomaterials show great potential for applications that require multiphoton absorbance, such as bioimaging and photodynamic therapy. Future studies will explore alternative dopant materials and SNC shapes that may offer greater flexibility with modulating the LSPR resonance wavelength to match the absorption edge of CuS.

ASSOCIATED CONTENT

Supporting Information

The Supporting Information is available free of charge on the [ACS Publications website](#) at DOI: [10.1021/acsp Photonics.6b00037](https://doi.org/10.1021/acsp Photonics.6b00037).

Emission, extinction, and XRD spectra of Se-doped copper sulfide nanocrystals; plasmon resonance as a function of Se content and a summary of morphology and optical properties of Se-doped copper sulfide nanocrystals; summary of equations and method in calculating two-photon action cross sections ([PDF](#))

AUTHOR INFORMATION

Corresponding Author

*E-mail (A. R. Tao): atao@ucsd.edu. Phone: (858) 822-4237. Fax: (858) 534-9533.

Author Contributions

[‡]B. C. Marin and S.-W. Hsu contributed equally to this work.

Notes

The authors declare no competing financial interest.

ACKNOWLEDGMENTS

This work is funded by a grant from the National Science Foundation (CHE, Award No. 1508755). The authors would like to thank the UCSD School of Medicine Microscopy Core for the use of their facility and acknowledge its supporting grant, NS047101. A.R.T. gratefully acknowledges financial support from the Arthur P. Sloan Foundation.

REFERENCES

- (1) Larson, D. R.; Zipfel, W. R.; Williams, R. M.; Clark, S. W.; Bruchez, M. P.; Wise, F. W.; Webb, W. W. Water-Soluble Quantum Dots for Multiphoton Fluorescence Imaging in Vivo. *Science* **2003**, *300*, 1434–1436.
- (2) Michalet, X.; Pinaud, F. F.; Bentolila, L. A.; Tsay, J. M.; Doose, S.; Li, J. J.; Sundaresan, G.; Wu, A. M.; Gambhir, S. S.; Weiss, S. Quantum Dots for Live Cell, in Vivo Imaging and Diagnostics. *Science* **2005**, *307*, 538–544.
- (3) Gao, X.; Yang, L.; Petros, J. A.; Marshall, F. F.; Simons, J. W.; Nie, S. In Vivo Molecular and Cellular Imaging with Quantum Dots. *Curr. Opin. Biotechnol.* **2005**, *16*, 63–72.
- (4) Liu, Q.; Guo, B.; Rao, Z.; Zhang, B.; Gong, J. R. Strong Two-Photon-Induced Fluorescence from Photostable, Biocompatible Nitrogen-Doped Graphene Quantum Dots for Cellular and Deep-Tissue Imaging. *Nano Lett.* **2013**, *13*, 2436–2441.
- (5) Gao, D.; Agayan, R. R.; Xu, H.; Philbert, M. A.; Kopelman, R. Nanoparticles for Two-Photon Photodynamic Therapy in Living Cells. *Nano Lett.* **2006**, *6*, 2383–2386.
- (6) Resch-Genger, U.; Grabolle, M.; Cavaliere-Jaricot, S.; Nitschke, R.; Nann, T. Quantum Dots versus Organic Dyes as Fluorescent Labels. *Nat. Methods* **2008**, *5*, 763–775.
- (7) Wang, B. G.; Konig, K.; Halhuber, K. J. Two-Photon Microscopy of Deep Intravital Tissues and Its Merits in Clinical Research. *J. Microsc.* **2010**, *238* (1), 1–20.
- (8) Pu, S. C.; Yang, M. J.; Hsu, C. C.; Lai, C. W.; Hsieh, C. C.; Lin, S. H.; Cheng, Y. M.; Chou, P. T. The Empirical Correlation Between Size and Two-Photon Absorption Cross Section of CdSe and CdTe Quantum Dots. *Small* **2006**, *2*, 1308–1313.
- (9) Padilha, L.; Fu, J.; Hagan, D.; Van Stryland, E.; Cesar, C.; Barbosa, L.; Cruz, C. Two-Photon Absorption in CdTe Quantum Dots. *Opt. Express* **2005**, *13*, 6460–6467.
- (10) Durr, N. J.; Larson, T.; Smith, D. K.; Korgel, B. A.; Ben-Yakar, A. Two-Photon Luminescence Imaging of Cancer Cells Using Molecularly Targeted Gold Nanorods. *Nano Lett.* **2009**, *7*, 941–945.
- (11) Wang, H.; Huff, T. B.; Zweifel, D. A.; He, W.; Low, P. S.; Wei, A.; Cheng, J. X. In Vitro and in Vivo Two-Photon Luminescence Imaging of Single Gold Nanorods. *Proc. Natl. Acad. Sci. U. S. A.* **2005**, *102*, 15752–15756.
- (12) Park, J.; Estrada, A.; Sharp, K.; Sang, K.; Schwartz, J. A.; Smith, D. K.; Coleman, C.; Payne, J. D.; Korgel, B. A.; Dunn, A. K.; Tunnell, J. W. Imaging of Tumors Using Near-Infrared Excited Gold Nanoshells. *Opt. Express* **2008**, *16*, 214–221.
- (13) Yuan, H.; Khoury, C. G.; Hwang, H.; Wilson, C. M.; Grant, G. A.; Vo-Dinh, T. Gold Nanostars: Surfactant-Free Synthesis, 3D Modelling, and Two-Photon Photoluminescence Imaging. *Nanotechnology* **2012**, *23*, 075102.
- (14) Medintz, I. L.; Uyeda, H. T.; Goldman, E. R.; Mattoussi, H. Quantum Dot Bioconjugates for Imaging, Labelling and Sensing. *Nat. Mater.* **2005**, *4*, 435–446.
- (15) Hwang, S.-Y.; Tao, A. R. Biofunctionalization of Gold Nanorods. *Pure Appl. Chem.* **2010**, *83*, 233–241.
- (16) Ueno, K.; Juodkazy, S.; Shibuya, T.; Yokota, Y.; Mizeikis, V.; Sasaki, K.; Misawa, H. Nanoparticle Plasmon-Assisted Two-Photon Polymerization Induced by Incoherent Excitation Source. *J. Am. Chem. Soc.* **2008**, *130*, 6928–6929.

- (17) Alkilany, A. M.; Thompson, L. B.; Boulos, S. P.; Sisco, P. N.; Murphy, C. J. Gold Nanorods: Their Potential for Photothermal Therapeutics and Drug Delivery, Tempered by the Complexity of Their Biological Interactions. *Adv. Drug Delivery Rev.* **2012**, *64*, 190–199.
- (18) Bouhelier, A.; Bachelot, R.; Lerondel, G.; Kostcheev, S.; Royer, P.; Wiederrecht, G. P. Surface Plasmon Characteristics of Tunable Photoluminescence in Single Gold Nanorods. *Phys. Rev. Lett.* **2005**, *95* (26), 267405.
- (19) Kano, H.; Kawata, S. Two-Photon-Excited Fluorescence Enhanced by a Surface Plasmon. *Opt. Lett.* **1996**, *21*, 1848–1850.
- (20) Lakowicz, J. R. Plasmonics in Biology and Plasmon-Controlled Fluorescence. *Plasmonics* **2006**, *1*, 5–33.
- (21) Zhao, T.; Wu, H.; Yao, S. Q.; Xu, Q.-H.; Xu, G. Q. Nanocomposites Containing Gold Nanorods and Porphyrin-Doped Mesoporous Silica with Dual Capability of Two-Photon Imaging and Photosensitization. *Langmuir* **2010**, *26*, 14937–14942.
- (22) Luther, J. M.; Jain, P. K.; Ewers, T.; Alivisatos, A. P. Localized Surface Plasmon Resonances Arising from Free Carriers in Doped Quantum Dots. *Nat. Mater.* **2011**, *10*, 361–366.
- (23) Zhao, Y.; Pan, H.; Lou, Y.; Qiu, X.; Zhu, J.; Burda, C. Plasmonic Cu_{2-x}S Nanocrystals: Optical and Structural Properties of Copper-Deficient Copper (I) Sulfides. *J. Am. Chem. Soc.* **2009**, *131*, 4253–4261.
- (24) Hsu, S. W.; On, K.; Tao, A. R. Localized Surface Plasmon Resonances of Anisotropic Semiconductor Nanocrystals. *J. Am. Chem. Soc.* **2011**, *133*, 19072–19075.
- (25) Hsu, S.-W.; Bryks, W.; Tao, A. R. Effects of Carrier Density and Shape on the Localized Surface Plasmon Resonances of Cu_{2-x}S Nanodisks. *Chem. Mater.* **2012**, *24*, 3765–3771.
- (26) Hsu, S. W.; Ngo, C.; Tao, A. R. Tunable and Directional Plasmonic Coupling within Semiconductor Nanodisk Assemblies. *Nano Lett.* **2014**, *14*, 2372–2380.
- (27) Ku, G.; Zhou, M.; Song, S.; Huang, Q.; Hazle, J.; Li, C. Copper Sulfide Nanoparticles as a New Class of Photoacoustic Contrast Agent for Deep Tissue Imaging at 1064 nm. *ACS Nano* **2013**, *6*, 7489–7496.
- (28) Liang, W.; Whangbo, M. H. Conductivity Anisotropy and Structural Phase Transition in Covellite CuS. *Solid State Commun.* **1993**, *85*, 405–408.
- (29) Grozdanov, I.; Najdoski, M. Optical and Electrical Properties of Copper Sulfide Films of Variable Composition. *J. Solid State Chem.* **1995**, *114*, 469–475.
- (30) Wu, C.; Szymanski, C.; Cain, Z.; McNeill, J. Conjugated Polymer Dots for Multiphoton Fluorescence Imaging. *J. Am. Chem. Soc.* **2007**, *129*, 12904–12905.
- (31) Denk, W.; Strickler, J. H.; Webb, W. W. Two-Photon Laser Scanning Fluorescence Microscopy. *Science* **1990**, *248*, 73–76.
- (32) Wang, Y. L.; Mohammadi Estakhri, N.; Johnson, A.; Li, H. Y.; Xu, L. X.; Zhang, Z.; Alù, A.; Wang, Q. Q.; Shih, C. K. Tailoring Plasmonic Enhanced Upconversion in Single NaYF₄:Yb³⁺/Er³⁺ Nanocrystals. *Sci. Rep.* **2015**, *5*, 10196.
- (33) Xu, C.; Webb, W. W. Measurement of Two-Photon Excitation Cross Sections of Molecular Fluorophores with Data from 690 to 1050 nm. *J. Opt. Soc. Am. B* **1996**, *13*, 481.
- (34) Albota, M. A.; Xu, C.; Webb, W. W. Two-Photon Fluorescence Excitation Cross Sections of Biomolecular Probes from 690 to 960 nm. *Appl. Opt.* **1998**, *37*, 7352–7356.
- (35) Wang, X.; Tian, X.; Zhang, Q.; Sun, P.; Wu, J.; Zhou, H.; Jin, B.; Yang, J.; Zhang, S.; Wang, C.; Tao, X.; Jiang, M.; Tian, Y. Assembly, Two-Photon Absorption, and Bioimaging of Living Cells of a Cuprous Cluster. *Chem. Mater.* **2012**, *24*, 954–961.
- (36) Wang, T.; Halaney, D.; Ho, D.; Feldman, M. D.; Milner, T. E. Two-Photon Luminescence Properties of Gold Nanorods. *Biomed. Opt. Express* **2013**, *4*, 584–595.